Original article

Investigation of the Effect of Flow Dynamics and on-chip Magnet Distance on Magnetic Particles in Microfluidic Channels

Zahra Zendeh [a], Reza Didarian [b], Sevda Zourazema [a], Fatemeh Shahriyari [c],

Beyza Dağhan [b], Emrehan Gürsoy [d], Mesut Bora Akdoğan [b], Kamil Arslan [b],

Leyla Didem Kozacı [c] & Fatma Doğan Güzel [b, *]

[a] Department of Translational Medicine, Faculty of Medicine,, Ankara Yildirim Beyazit University, Ankara, Türkiye
[b] Department of Mechanical Engineering, Ankara Yildirim Beyazit University, Ankara, Türkiye
[c] Department of Biochemistry, Faculty of Medicine, Ankara Yildirim Beyazit University, Ankara, Türkiye
[d] Kardemir Karabük Iron Steel Industry Trade Co. Inc. Karabük, Türkiye

Abstract

This study explores the dynamics of magnetic microparticles in a magnet-integrated microfluidic chip, examining the effects of magnet distance and flow rate on particle motion. The integrated system enables compact, on-chip magnetophoresis for separating biologically important molecules and microorganisms. Experiments used Neodymium (NdFeB) magnets positioned at 10, 11, and 12 mm from the channel and flow rates of 0.5, 0.7, and 1 µl/min. At 10 mm, the magnetic field strongly influenced particle motion, causing accumulation near the channel walls, especially at lower flow rates. As the distance increased, drag forces dominated, reducing magnetic control. The highest particle accumulation (14.94%) occurred at 10 mm with a 0.5 µl/min flow rate, while the highest percentage of particles exiting the upper outlet (60.18%) was observed at 11 mm with 0.7 µl/min. These findings provide insights into the interplay between magnetic fields, hydrodynamic forces, and particle dynamics in microfluidic environments. They have potential applications in targeted drug delivery, diagnostics, and lab-on-a-chip technologies, where precise particle control is crucial for optimizing performance.

Keywords: Iron Oxide Microparticles, Microfluidic Systems, Polydimethylsiloxane (PDMS), Magnetic Forces.

---

* Corresponding author:

Fatma Doğan Güzel, Department of Mechanical Engineering, Ankara Yildirim Beyazit University, Ankara, Türkiye.
Email: fdogan@aybu.edu.tr

INTRODUCTION

In recent years some research has been done to investigate the mechanical behavior of micro and nanoparticles in fluids [1-3]. Alongside mathematical studies and modeling, research on the movement paths of particles in microfluidics has progressed to the experimental stage. The validation of predicted particle movement through experimental studies has been emphasized, as particle tracking in microfluidics cannot be fully understood from a single perspective, making real experiments necessary. In recent advancements, Zeng et al. proposed an innovative microfluidic system utilizing an ultra-strong magnetic field for the label-free separation of nanoparticles [4]. This pioneering approach significantly enhances the precision and efficiency of nanoparticle separation, which is critical for various biomedical applications. Numerous studies have demonstrated that the optimal targeting and increased efficacy of magnetic drug delivery systems (MDDS) are closely linked to the precise control of particle trajectories within the delivery environment. Over the past decades, extensive research has been dedicated to understanding and improving magnetic drug targeting, with particular focus on the behavior of particles in magnetic fields. One of the core areas of MDDS research is the dynamics of particle movement under magnetic influence. Driscoll et al. conducted seminal research on the movement of magnetic drug carrier particles, examining the interplay between magnetic drag and Stokes forces [5]. Their findings provided foundational insights into how these forces can be manipulated to control particle movement. Building on this foundation, Liu et al. explored various strategies for concentrating magnetic particles within specific target areas by simulating a targeted drug delivery system [6]. Their research highlighted the potential for fine-tuning magnetic field parameters to achieve precise particle localization, thereby enhancing the effectiveness of drug delivery.

Magnetic fields possess a profound ability to manipulate and segregate particles within microchannels, offering significant advantages in fields such as biomedicine, microfluidics, and materials science. Diamagnetic particles, for instance, exhibit negative magnetophoresis, causing them to deflect across the channel due to the presence of an induced magnetic field gradient. This process enables the effective focusing and segregation of particles based on their sizes, facilitating precise manipulation [7]. Furthermore, magnetic particles tend to form chains and clusters under the influence of a rotating uniform magnetic field, allowing for their direction towards specific regions of the microchannel, either upper or lower [8]. The behavior of aggregation and flow of magnetic particles in microchannels is primarily dictated by the transverse magnetic field applied [9]. The ability to control and manage particles using external magnetic fields offers distinct advantages, such as precise manipulation and sorting capabilities that surpass traditional methods [10].

Microchannels, typically characterized by dimensions ranging from tens to hundreds of micrometers, provide a confined environment where the interplay between fluid flow and particle behavior can be meticulously controlled [10]. Upon exposure to magnetic fields, particles exhibit

distinct behaviors such as alignment, aggregation, or deviation, depending on their magnetic properties, the intensity of the field, and their orientation. Understanding these behaviors is crucial for advancing techniques in areas like drug delivery systems, lab-on-a-chip devices, and environmental monitoring sensors [7]. Microfluidic chips and lab-on-a-chip systems play an important role in advancing various fields, including engineering and medicine, by providing precise control over small liquid volumes and their effects on tiny particles, such as magnetic nanoparticles. These systems serve as efficient tools for the generation, manipulation, and evaluation of nanoparticles [11].

Various methodologies, such as the use of external magnets, integration of micro-coils, and the utilization of magnetic thin films, are employed in microfluidic techniques to regulate magnetic nanoparticles. These nanoparticles can be customized with surface modifications, including antibodies, oligonucleotides, and aptamers, to engage in specific interactions with target viruses or their components, thus facilitating detection [12]. The integration of magnetic nanoparticles and microfluidics is prominently demonstrated in lab-on-a-chip immunoassays, where superparamagnetic beads act as markers to facilitate the transport, separation, and categorization of different bead types [13]. Ongoing advancements include microfluidic magnetic separation, magnetic relaxation switch immunosensors that simplify handling and enhance sample detection signals using enzyme-assisted nanoparticles, and microfluidic nuclear magnetic resonance detection devices for the rapid identification of tumor markers [14].

The field of magnetic particle manipulation in lab-on-a-chip applications is rapidly evolving, presenting challenges associated with weak magnetic forces and particle surface interactions. Generally, the merging of microfluidics and magnetic nanoparticles supports significant advancements in biotechnology by enabling the development of sensitive, high-throughput, and portable instruments for contactless identification and handling of DNAs, RNAs, living cells, and viruses [11].

In this study, the primary objective is to conduct a comprehensive experimental examination of particle motion in microchannels under the influence of magnetic fields. Utilizing advanced imaging techniques and precise control of magnetic fields, this investigation aims to elucidate the dynamic phenomena and motion patterns exhibited by various particles. The study's goal is to understand the fundamental principles governing particle dynamics in microfluidic environments, which are crucial for fields such as biomedical engineering, targeted drug delivery, and lab-on-a-chip technologies. By methodically adjusting both the strength and orientation of the magnetic field, the aim is to gain new insights into the control and enhancement of particle movement within microchannels. The integration of magnetic field manipulation in microfluidic environments could revolutionize how we approach complex problems in diagnostics, treatment, and beyond. Such selective separation of magnetic particles in microfluidic chips will potentially be used for different applications in biomedical field.

EXPERIMENTAL SECTION

Materials

Iron oxide microparticles with a size of 2 μm (310069-25G) were purchased from Sigma-Aldrich (Wisconsin, USA). PDMS powder, SU-8 2050 light-sensitive polymer, and Propylene glycol methyl ether acetate (PGMEA) were purchased from Microchem company. Chemicals, including acetone, isopropanol (IPA), ethanol, and phosphate-buffered saline (PBS), were purchased from Merck. NdFeB permanent magnets (MOD1-20, 5 mm × 1.5 mm × 1 mm) were purchased from Magnet expert ltd company. Polyethylene tubing (with 0.38 mm ID, 1.09 mm OD) was purchased from Harvard Apparatus Company (USA). Acetate photomasks was fabricated by Çözüm Tanıtım (Turkey). The EUROMEX OXION INVERSO (Netherlands) inverted microscope was used to study the motion of magnetic nanoparticles within microfluidic chips.

Fabrication of microfluidic devices

Microfluidic chip templates were fabricated using the SU-8 2050 negative photoresist through a standard optical photolithography method [15,16]. Initially, a 3-inch silicon (Si) wafer was placed on a spin coater (Laurell, Model WS-650MZ-23NPPB, USA). The photoresist was spin-coated onto the wafer at 500 rpm for 10 seconds and then at 3000 rpm for 25 seconds to create a uniform photoresist layer. The Si wafer underwent a soft bake at 65 °C for 3 minutes, followed by a hard bake at 95 °C for 7 minutes to solidify the resist. Subsequently, a photomask containing the desired microchannel design was aligned with the coated wafer, and the wafer was exposed to ultraviolet (UV) light for 5 minutes using a handmade UV exposure setup with a dose of 1 mJ/min [17,18]. This UV exposure facilitated the transfer of the microchannel pattern onto the photoresist layer. Post-exposure baking was performed by heating the wafer at 65 °C for 1 minute and 95 °C for 7 minutes, ensuring the photoresist was fully developed. After cooling the wafer to room temperature, it was immersed in 50 ml of PGMEA (propylene glycol monomethyl ether acetate) and gently agitated for 5 minutes to remove the unexposed photoresist. The wafer was then rinsed with isopropanol and deionized water for approximately 10 seconds to halt the development process and remove any residual PGMEA. The wafer was subsequently dried using nitrogen gas [19].

Next, NdFeB magnets were strategically placed at distances of 10, 11, and 12 mm from the center of the microchannel in three different chips, respectively. The alignment of these magnets was verified using a microscope, ensuring precise placement within the chip structure. The fabrication of the microfluidic chip continued with the preparation of polydimethylsiloxane (PDMS) molds. PDMS and cross linker (Sylgard 184 silicon elastomer base and Sylgard 184 silicon elastomer curing agent, Dow Corning, USA) were thoroughly mixed in a 10:1 ratio for 3 minutes. The mixture was then poured onto the prepared template and subjected to vacuuming in a desiccator for 20 minutes to remove any

entrapped air bubbles. To cure the PDMS, the template was heated at 80 °C for 2 hours. Following the curing process, the solidified PDMS layer, now containing the microfluidic channels, was carefully peeled off from the silicon template. After cutting and perforating the PDMS mold to form inlet and outlet ports, the magnets were attached to the PDMS using paper adhesive for subsequent plasma treatment. For the bonding process, the PDMS and glass slide were exposed to oxygen plasma using a custom-built plasma device. The PDMS mold was then aligned and bonded to the plasma-treated glass slide to complete the microfluidic chip assembly. Prior to bonding, the glass surface was meticulously cleaned using isopropyl alcohol (IPA), acetone, and deionized water to ensure a strong bond and avoid contamination. The final microfluidic chip, now equipped with integrated magnets and precisely engineered channel architecture, was ready for the study of magnetic nanoparticle motion within the microchannels. Figure 1 shows the schematic of the microfluidic chip designed and used in this study. Magnet built-in microfluidic channel consisting of 1 inlet and two outlets with particular dimensions and distances in between is implemented experimentally. Various flow rates and magnet distances to the channel are studied to understand the dynamic force relations acting on the particle.
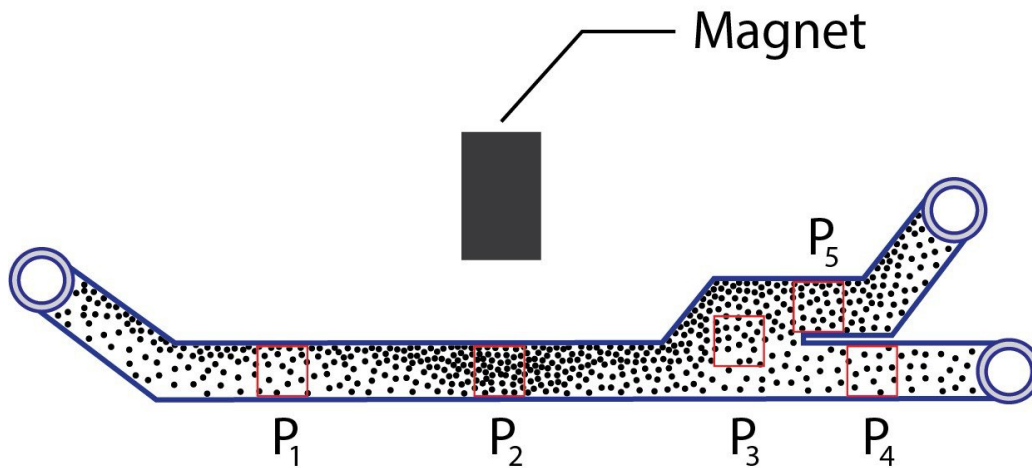

Figure 1. Schematic of the designed microfluidic system and channel sections observed during experiments. P1: Before magnet, P2: Magnet area, P3: After magnet, P4: Upper outlet, P5: Lower outlet.

Particle trajectory experiments

The particle trajectory experiments were divided into two main setups. First, after cleaning the microchannels with deionized water, 0.1 mg of iron oxide microparticles was added to 10 ml of pure water for the first experiment, and to 10 ml of fresh blood plasma for the second experiment. The microparticles were dispersed using an ultrasonic bath for 45 minutes. The solution was then injected into the microchannel using syringe pumps (New Era Pump Systems, NE-4002X, USA). Polyethylene

tubing was used for both the inlet and outlet. An optical microscope (Euromex Oxion Inverso) was employed to observe the movement of the particles (Figure 2).
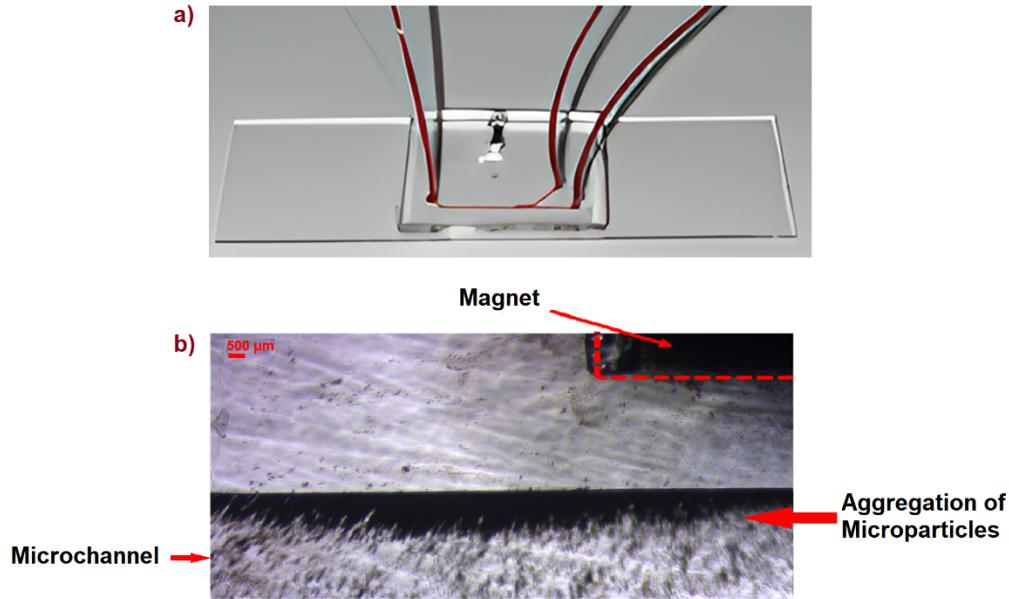

Figure 2. (a) Image of the designed chip; (b) Microscope image of the microchannel showing the collection of microparticles in front of the magnet at a flow rate of 0.5 µl/min.

Various experiments were conducted to assess the effects of key parameters, such as flow rate and the distance between the channel and the magnet (Table 1). Once a steady-state condition was achieved after 10 min, the movement of the particles was monitored and recorded using a CCD camera. The images obtained at different flow rates and varying distances between the microchannel and the magnets were analyzed and interpreted using the ImageJ software.

Table 1. Experiments were conducted at varying flow rates and distances between the magnet chips. Each distance and flow rate combination were tested with 6 repetitions, and the average results were calculated.

Magnet Distance (mm)	Flow Rate (µl /min)		
10	0.5	0.7	1
11	0.5	0.7	1
12	0.5	0.7	1

Simulation studies

In this section particle movement has been studied and optimized in a fluid. The analysis has been performed via ANSYS Fluent 2024 R1 software. In the realm of numerical solution, the decision to employ the *SIMPLE* algorithm for Pressure-Velocity Coupling has been made based on its superior

iteration speed when compared to the *PISO* and *COUPLED* algorithms. This choice has been driven by its ability to enforce continuity, a crucial aspect of the present study. The *SIMPLE* algorithm establishes a relation between velocity and pressure corrections, yielding a pressure gradient. Additionally, Spatial Discretization for Gradient, Pressure, and Momentum solutions involved the application of Least Squares Cell-Based and Second Order Upwind methods, respectively. The Second Order Scheme has been also utilized to refine results in terms of pressure calculation. The Second Order Upwind Scheme has also been selected for the discretization of Momentum and Energy equations, ensuring reliable results.

RESULTS and DISCUSSION

In this study, a magnet is integrated onto PDMS chip to obtain a compact potential separation device for future applications. The effect of magnet distance (10, 11 and 12 mm) and varying flow rates (0.5, 0.7, and 1 µl/min) on micron-size magnetic particle moving in the microfluidic channels are investigated experimentally. It is aimed that the interplay between magnetic forces and hydrodynamic forces reveals basics technical information for researchers of on-chip magnetophoresis studies. The migration of particles under an external magnetic field depends on the balance of forces acting on them (Figure 3). The primary forces influencing the particle are the inertial force ($m_p d v / dt$), the magnetic force (F_m), and the fluid drag force (F_d). In a shallow channel and an incompressible fluid, gravitational force (F_g) and Brownian force (F_b) have minimal effect on the particles and are therefore excluded from the calculations. For simplicity, total acting forces is shown by;

$$m_p \frac{dv}{dt} = F_m + F_d \qquad (1)$$

Where m_p is the mass of the particle, v is the velocity of the particle, F_m is the magnetic force, and F_d is the viscous drag force. According to the Stokes law, the viscous drag force is determined as;

$$F_d = \frac{1}{\tau p} mp(uf - v) \qquad (2)$$

Where τp (s) is the velocity response time of the particle, represented by;

$$\tau p = \frac{\rho p \ x \ dp^2}{18\mu} \qquad (3)$$

Where ρp and dp are the density and the diameter of the particle, respectively, μ is the fluid viscosity. Magnetophoretic force acting on the particle in a fluidic medium is then represented by;

$$F_m = (V(\chi - \chi_m)/\mu_0) \ x \ (\nabla . B)B \qquad (4)$$

Where μ_0 is magnetic permeability of the air, V *is* particle volume, χ is magnetic susceptibility, χ_m is the susceptibility of the surrounding medium, and $\nabla . B$ is field gradient of the magnetic flux density. As clearly seen, the magnetic force acting on the particles depends on the shape of the magnet and the distance to the microchannel -whether it is mobile or not- and the surrounding

medium and the particle size. As seen clearly there many forces and factors involved on the particle movement, and this study narrowed down the parameters to magnet distance and flow rates.
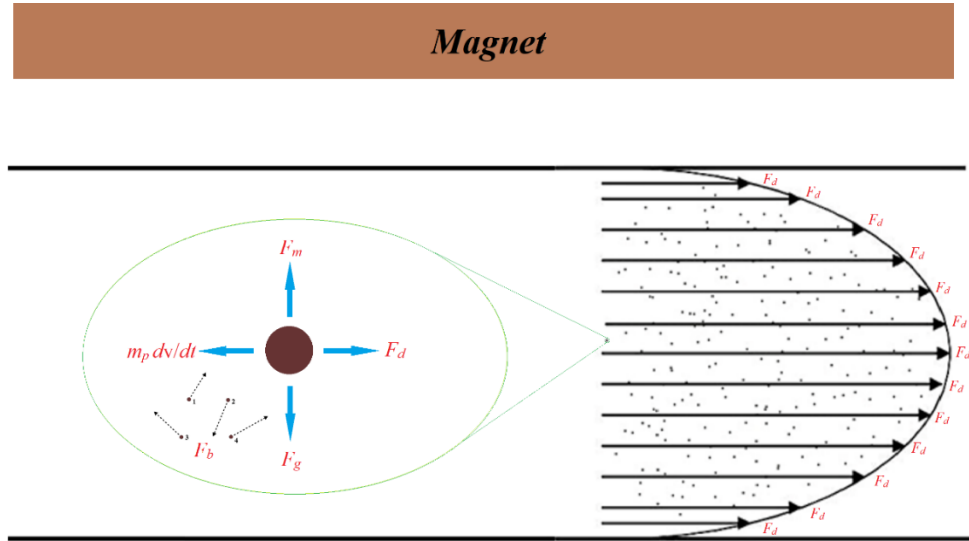

Figure 3. Schematic of forces acting on magnetic particles flowing through a microchannel. Inertial force ($m_p dv/dt$), Magnetic force (F_m), Fluid drag force (F_d), Gravitational force (F_g) and Brownian force (F_b).

Particles dispersed in water are subjected to both magnetic and drag forces at varying flow velocities as they enter the microchannel. At a higher flow rate of 1 µl/min, the drag force dominates, resulting in a backflow effect where most particles are directed towards the lower outlet. As the flow rate decreases to 0.7 and 0.5 µl/min, the particles begin to shift towards the upper outlet. This is because the magnetic force primarily acts on the particles for a longer duration, allowing it to have a greater impact on their trajectory. At the lowest flow rate of 0.5 µl/min, marginal movement occurs, with many particles moving towards the walls of the channel. This is a result of the extended exposure to the magnetic force, which becomes more prominent as the flow rate slows, making the magnetic influence the dominant force in particle movement. At the higher flow rate of 1 µl/min, the particles show more random motion, indicating that their paths are less influenced by the magnetic field. This can be explained by the principle of linear momentum conservation: at higher velocities, particles with the same mass possess greater linear momentum, meaning that more force is required to alter their path. Consequently, particles at lower flow rates have reduced momentum and are more easily deflected by the magnetic field, causing them to deviate more quickly from their initial trajectory and move towards the upper part of the channel. Interestingly, at a flow rate of 1 µl/min, fewer particles accumulate in front of the magnet, while reducing the flow rate to 0.5 µl/min results in a noticeable increase in particle collection around the magnet. This happens because the longer the particles are exposed to the magnetic force, the greater the lateral displacement, especially at lower flow rates where the drag force is weaker.

Furthermore, at a short distance of 10 mm between the magnet and the channel, the magnetic force significantly influences the particles, causing them to suspend and agglomerate near the magnet (Figure 2b). This is due to the reduced linear momentum and increased magnetic force acting on the particles at close range. When the distance is increased to 11 mm, the particles are able to move more freely, reducing agglomeration, as the magnetic influence weakens slightly with distance. This highlights the delicate balance between flow rate, magnetic force affected by the distance between the magnet and the channel, all of which determine the behavior of particles in such systems.

At a distance of 10 mm between the magnet and the channel, and at a lower flow rate of 0.5 µl/min, the magnetic force exerts a strong influence on the particles. Most of them tend to adhere to the upper wall of the channel due to the reduced drag force, which allows the magnetic force to dominate. By increasing the flow rate to 0.7 µl/min, the movement of particles remains stable, with changes in their position along the channel and a deviation toward the upper outlet. However, at the highest flow rate of 1 µl/min, the magnetic force becomes less dominant, and the particles begin to tilt slightly towards the channel wall, though the movement remains somewhat random as the increased drag force counteracts the magnetic influence (Figure 4 upper images).

When the magnet is placed at a distance of 11 mm from the channel, the behavior of the particles changes significantly. At the lowest flow rate of 0.5 µl/min, the magnetic force still plays a significant role, and the particles are drawn toward the wall. However, as the flow rate increases to 0.7 µl/min, the drag force starts to outweigh the magnetic force, causing the particles to move away from the wall and more towards the center of the channel. Notably, as the particles pass in front of the magnet, they experience a brief decrease in speed, followed by an increase, as the magnetic field loses its grip and the particles are propelled forward by the flow. At the highest flow rate of 1 µl/min, particles again tend to stay closer to the walls, but the overall movement becomes more stable, with fewer deviations from their path (Figure 4 middle images).

At a distance of 12 mm, the control of the magnetic field on the particles is even weaker. At the lowest flow rate of 0.5 µl/min, the particles gradually move away from the wall and along the channel. As the flow rate increases to 0.7 and 1 µl/min, the particles are significantly affected by the flow, deviating from the upper wall of the channel toward the center and exhibiting random movement. Their velocities follow an oscillatory pattern, especially at the highest flow rates, reflecting weak magnetic control and increasing drag dominance (Figure 4 below images). The higher separation is seemingly observed with 0,7 µl/min at a distance of 11 mm.
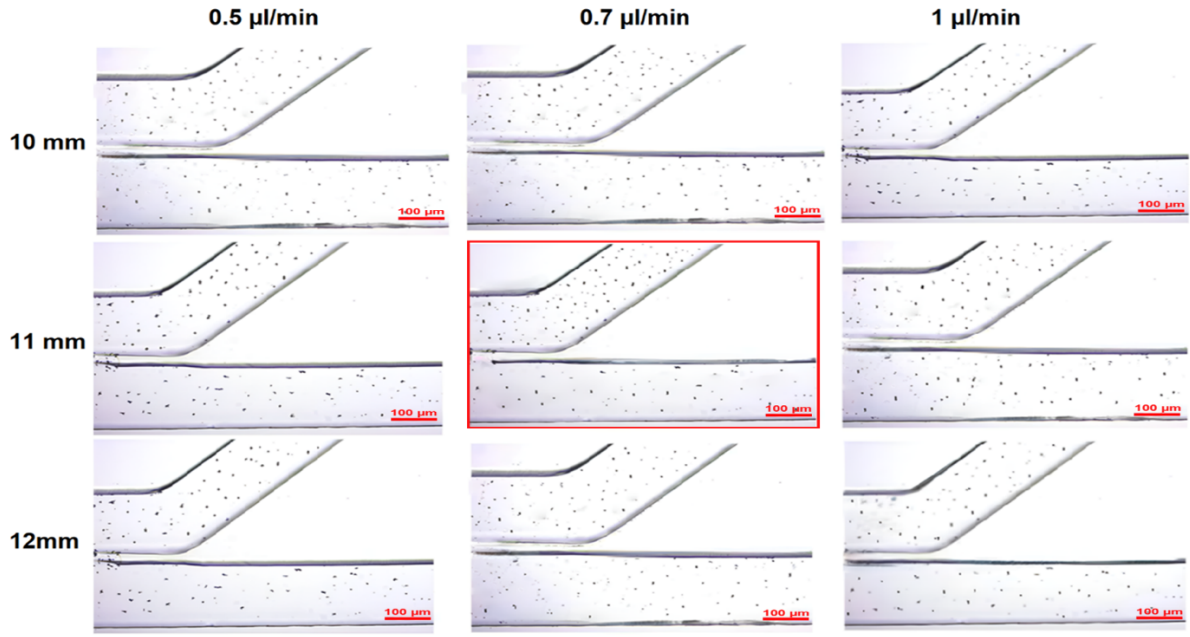
Figure 4. Photographs showing the movement of microparticles and their orientation toward the outlets at distances of 10, 11, and 12 mm from the magnet, with flow rates of 0.5, 0.7, and 1 µl/min.

Figure 5 shows changes obtained from six repetitions of experiments for each flow rate and distance between the magnet and the microchannel. The analysis indicates that as the distance between the magnet and the channel increases, the magnetic field's influence on the particles diminishes. At shorter distances (10 mm), the magnetic force is strong enough to significantly impact particle movement, pulling them toward the channel walls, especially at lower flow rates, leading to increased microparticle accumulation near the magnet. However, as the distance increases to 11 and 12 mm, the particles are more affected by the drag force from higher flow rates, resulting in smoother motion and fewer deviations. At higher flow rates, the particles' velocity and linear momentum become more dominant, reducing the effect of the magnetic field on their movement. To numerically represent the separation efficiency, percentage changes is calculated using the expression below;

$$\%Separation\ Efficiency\ (SE) = \frac{Number\ of\ Target\ Particles\ at\ each\ outlet}{Total\ Particles} \times 100 \quad (5)$$
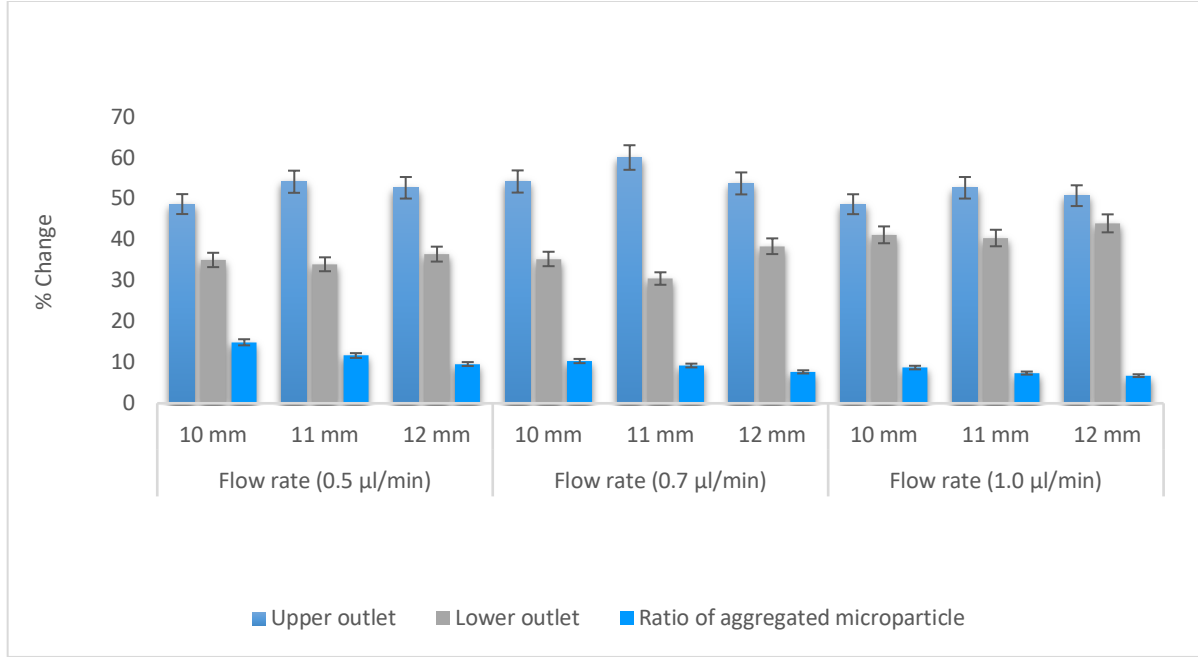
Figure 5. Comparison of the kinetic properties of magnetic microparticles in a microfluidic chip: percentage values of high and low output, and the amount of aggregation at different flow rates and varying distances of the magnet from the microchannel.

5 different positions are considered for calculations: P1; main channel entry, P2; main channel exit, P3; widened region, P4; upper outlet, P5; lower outlet. The main comparison is made between the number of particles entering the channel (P1) and observed in the outlets at the given positions (P4 and P5). As shown in Figure 5, the highest percentage of microparticles exiting from the upper outlet (60.18%) occurs at a distance of 11 mm from the magnet with a flow rate of 0.7 µl/min. Also the highest microparticle accumulation (14.94%) occurs at a 10 mm distance and a flow rate of 0.5 µl/min. The results show that the optimum separation efficiency, as supported by the optical observations, is obtained from 11 mm magnet distance and 0,7 µl/min. This is direct consequence of the balanced force play acting on the particles. As demonstrated by Eshaghi et al., close proximity to a strong magnetic field optimizes particle sorting and alignment, corroborating our findings that magnet distance affects the particle manipulation [7]. Driscoll et al. demonstrated that well-controlled flow rates and magnetic forces can drive predictable particle motion in microfluidic settings [5]. Notably, at lower flow rates, particles exhibited higher retention near the magnets, allowing for targeted separation in biological fluids, a key benefit in biomedical microdevices where selective particle retention is crucial.

In our study, the outlet design is particularly chosen as such to enhance the separation efficiency. In classical channel designs, the outlets are separated straight after the main channel with no specific channel geometry. The main channel is 10 mm long and 250 µm wide. The width of outlet channels is widened to 600 µm (P3 region) before they are separated with an initial gap of 75 µm-wide. This area

is about 3 mm long and facilitates the manipulation of particles towards upper outlet. Cao and colleagues have further highlighted the influence of device geometry on magnetic particle separation efficiency [8]. Their study illustrates that microdevice design particularly channel width, depth, magnetic field strength, and outlet positioning directly impacts the behavior of particles in continuous-flow systems. This supports the application of optimized geometrical and field parameters to increase separation efficiency in lab-on-a-chip systems and microfluidic diagnostics.

The movement of iron oxide particles in blood at same chosen flow rates were also studied. At lower flow rates, a greater number of particles were visible in the images. Experimental observations revealed that at a 10 mm distance and a flow rate of 0.5 µl/min, due to reduce linear momentum, more particles adhered to the channel walls, and were more likely to settle in the blood. As the distance increased to 11 and 12 mm, more particles moved toward the center of the channel, away from the walls, as the magnetic force acting on the particle is weakened. Additionally, it was observed that at the increased distance, most of the particles at a flow rate of 0.5 µl/min moved towards both outlets. These results highlight the influence of both flow rate and magnet distance on the behavior of iron oxide particles in blood flow, with closer distances enhancing wall adherence and longer distances promoting central movement. As a result, it can be stated that there was no significant difference in particle movement toward the outlets when using either water or blood plasma. Although the dynamic viscosity of the fluid was expected to influence particle movement, this was not observed in this study. The reason why dynamic viscosity did not have an observable effect is thought to be that the viscosity of prepared blood plasma (1.2 mPa·s) is only slightly higher than that of water (1.002 mPa·s), and this difference is not large enough to cause a significant change in particle movement.

We also simulated the effective magnetic field and flow dynamics on the microfluidic chip design in question. Various calculations and analyses were performed to ensure accurate results and detailed insights. The continuity equation given in Equation (6).

$$\nabla . \vec{V} = 0 \qquad\qquad (6)$$

Although the computational domain has the external force of Magnetic Field (MF), no change is not seen in the continuity equation. However, the momentum equation receives the Lorentz force component given in Equation (7) with the application of MF.

$$(\vec{V}.\nabla)\vec{V} = -\frac{1}{\rho}\nabla\dot{p} + \nu\nabla^2\vec{V} + g + \frac{1}{\rho}\vec{F} \qquad (7)$$

The distinct physical phenomena addressed by the Lorentz force expressed in Equation (8) and momentum equations find common ground within the realm of MHD. The Lorentz force specifically accounts for the movement of magnetic particles interacting with MFs, while the momentum equation delineates the motion of a working fluid, incorporating factors such as pressure, viscosity, and gravity.

In the application of MHD to the magnetizable fluid, magnetic conductive particles get velocity (V) and consequently momentum due to the MF.

Thus, the Lorentz force can be interpreted as a change in momentum and incorporated into the momentum equation. Furthermore, the counteractive impact of the Lorentz force on the flow can be determined through specific procedures.

$$\vec{F} = \vec{j} \, x \, \vec{B} \qquad (8)$$

Where $\vec{j} \, (A/m^2)$ describes the current density given in Equation (9) and obtained from Ohm's law. $\vec{B} \, (T)$ denotes MF strength acquired from Maxwell's equations.

$$\vec{j} = \sigma(\vec{E} + \vec{V} x \overrightarrow{B}) \qquad (9)$$

Where σ (*S/m*) shows the electrical conductivity of fluid, *E* (*V/m*) symbolizes the electrical field, and *V* (*m/s*) identify velocity of working fluid, respectively. In this scope, Ohm's law and Maxwell's equations derive the *MHD* equation given in Equation (10).

$$\left(\vec{V}.\nabla\right)\vec{B} = \frac{1}{\mu_{MF}\sigma}\nabla^2\vec{B} + \left(\vec{B}.\nabla\right)\vec{V} \qquad (10)$$

The analyses have been conducted for single-phase assumption; energy equation employed in numerical solutions for this assumption is denoted by Equation (11). Similar to the momentum equation, the generation of heat resulting from the application of a *MF* and the passage of a magnetic force through conductive materials have to be incorporated into the energy equation. This phenomenon, referred to in the literature as Joule Heating and added to right side of the equation within the framework of MHD.

$$\rho c_p \left(\left(\vec{V}.\nabla\right)T\right) = k\nabla^2 T + \mu_{MF}\phi + \frac{\overrightarrow{J^2}}{\sigma} \qquad (11)$$

in which Φ (*W/m3*) describes dissipation energy and identifies the consumed power for viscous forces.

A numerical model has been solved for three different velocity magnitudes. Figure 6 shows the velocity vectors for different velocity magnitudes. The effect of the magnetic field can be seen in these vector distributions. Also, flow slows near the magnetic field effect, and this condition changes the velocity magnitude in the branches of channels.
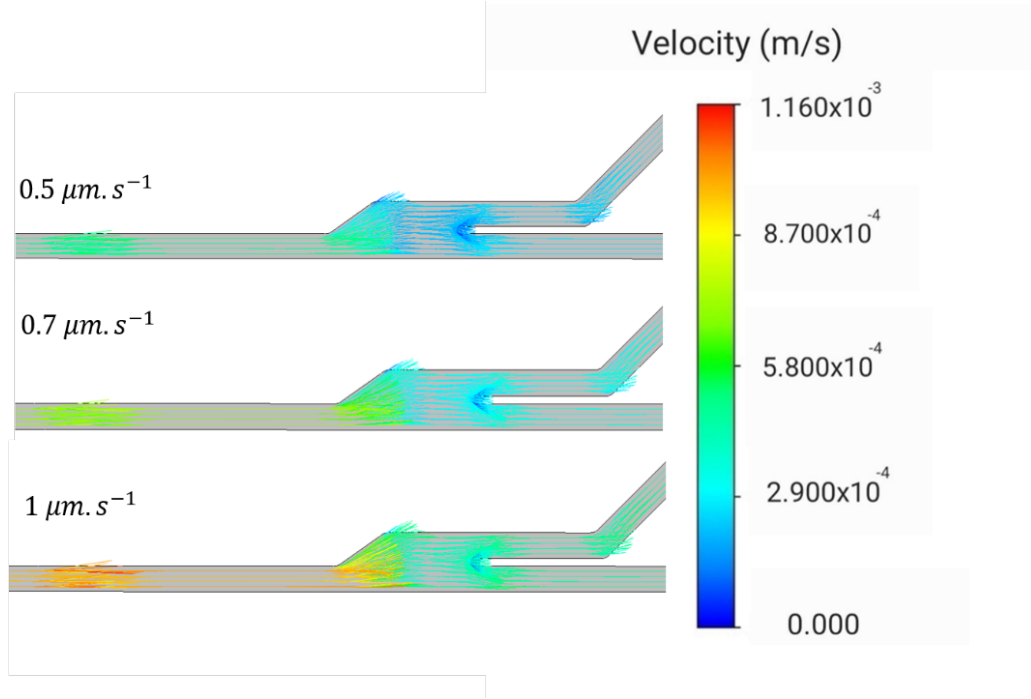
Figure 6. Simulation results obtained for 3 different flow rates.

Conclusion

This study demonstrates the on-chip integration of a magnet in microfluidic chips and experimentally investigates the critical interplay between magnetic field and flow dynamics actin upon magnetic particles moving within a specific design of microfluidic channels. At closer magnet distances, the magnetic force played a dominant role, causing particles to aggregate near the channel walls, especially at lower flow rates. At a magnet distance of 11 mm, 0.7 µl/min flow rate provides the optimum separation with about % 65 separation efficiency. When the flow rate is increased to 1 µl/min, the efficiency rate drops down. This work demonstrates the potential of microfluidic magnetic manipulation to refine particle behavior in small-scale devices, thus enhancing the functionality and efficiency of diagnostic and therapeutic microdevices. Future studies should investigate varying particle sizes and geometries in diverse biofluids, along with tailored microdevice designs to accommodate different biomedical applications, aiming to elevate performance in rapid diagnostics, drug delivery, and microfluidic-based analyses.

Acknowledgement

REFERENCES

[1] A. G. Arani, M. S. Zarei, Nonlocal vibration of Y-shaped CNT conveying nano-magnetic viscous fluid under magnetic field, Ain Shams Engineering Journal, 6(2), 565–575, 2015. https://doi.org/10.1016/j.asej.2014.11.012

[2] V. Garbin, J. C. Crocker, K. J. Stebe, Nanoparticles at fluid interfaces: Exploiting capping ligands to control adsorption, stability, and dynamics, Journal of Colloid and Interface Science, 387(1), 1–11, 2012. https://doi.org/10.1016/j.jcis.2012.06.052

[3] S. Oveissi, D. S. Toghraie, S. A. Eftekhari, Analysis of transverse vibrational response and instabilities of axially moving CNT conveying fluid, International Journal of Fluid Mechanics Research, 44(2), 123–135, 2017.

[4] L. Zeng, X. Chen, J. Du, Z. Yu, R. Zhang, Y. Zhang, H. Yang, Label-free separation of nanoscale particles by an ultrahigh gradient magnetic field in a microfluidic device, Nanoscale, 13(7), 4029–4037, 2021. https://doi.org/10.1039/D0NR08383F

[5] C. F. Driscoll, R. M. Morris, A. E. Senyei, K. J. Widder, G. S. Heller, Magnetic targeting of microspheres in blood flow, Microvascular Research, 27(3), 353–369, 1984. https://doi.org/10.1016/0026-2862(84)90065-7

[6] Y. L. Liu, D. Chen, P. Shang, D. C. Yin, A review of magnet systems for targeted drug delivery, Journal of Controlled Release, 302, 90–104, 2019. https://doi.org/10.1016/j.jconrel.2019.03.031

[7] M. Eshaghi, M. Nazari, M. M. Shahmardan, M. Ramezani, V. Mashayekhi, Particle separation in a microchannel by applying magnetic fields and Nickel Sputtering, Journal of Magnetism and Magnetic Materials, 514, 167121, 2020. https://doi.org/10.1016/j.jmmm.2020.167121

[8] Q. Cao, X. Han, L. Li, Configurations and control of magnetic fields for manipulating magnetic particles in microfluidic applications: magnet systems and manipulation mechanisms, Lab on a Chip, 14(15), 2762–2777, 2014. https://doi.org/10.1039/C4LC00367E

[9] S. Varela, A. Rivas, A. Vernet, J. Pallarès, Experimental study of the deposition of magnetic particles on the walls of microchannels, Micromachines, 12(6), 712, 2021. https://doi.org/10.3390/mi12060712

[10] A. Surpi, T. Shelyakova, M. Murgia, J. Rivas, Y. Piñeiro, P. Greco, M. Fini, V. A. Dediu, Versatile magnetic configuration for the control and manipulation of superparamagnetic nanoparticles, Scientific Reports, 13(1), 5301, 2023. https://doi.org/10.1038/s41598-023-32299-9

[11] R. Abedini-Nassab, M. Pouryosef Miandoab, M. Şaşmaz, Microfluidic synthesis, control, and sensing of magnetic nanoparticles: A review, Micromachines, 12(7), 768, 2021. https://doi.org/10.3390/mi12070768

[12] N. Rezvani Jalal, P. Mehrbod, S. Shojaei, H. I. Labouta, P. Mokarram, A. Afkhami, T. Madrakian, M. Los, D. Schaafsma, M. Giersig, M. Ahmadi, S. Ghavami, Magnetic nanomaterials in microfluidic sensors for virus detection: A review, ACS Applied Nano Materials, 4(5), 4307–4328, 2021. https://doi.org/10.1021/acsanm.1c01077

[13] Ennen, A. Hütten, Magnetic nanoparticles meet microfluidics, Materials Today: Proceedings, 4(Suppl. 2), S160–S167, 2017. https://doi.org/10.1016/j.matpr.2017.09.181

[14] Z. Zhong, J. He, G. Li, L. Xia, Recent advances in magnetic nanoparticles-assisted microfluidic bioanalysis, Chemosensors, 11(3), 173, 2023. https://doi.org/10.3390/chemosensors11030173

[15] F. D. Güzel, B. Miles, Development of in-flow label-free single molecule sensors using planar solid-state nanopore integrated microfluidic devices, Micro & Nano Letters, 13(9), 1352–1357, 2018. https://doi.org/10.1049/mnl.2018.5206

[16] R. Didarian, A. Ebrahimi, H. Ghorbanpoor, H. Bagheroghli, F. D. Güzel, M. Farhadpour, N. Lotfibakhshayesh, H. Hashempour, H. Avci, On-chip microfluidic separation of cyclotides, Turkish Journal of Chemistry, 47(1), 253–262, 2023. https://doi.org/10.55730/1300-0527.3534

[17] H. Ghorbanpoor, A. Norouz Dizaji, I. Akcakoca, E. O. Blair, Y. Öztürk, P. J. Hoskisson, T. Kocagöz, H. Avcı, D. K. Corrigan, F. D. Güzel, A fully integrated rapid on-chip antibiotic susceptibility test – A case study for Mycobacterium smegmatis, Sensors and Actuators A: Physical, 339, 113515, 2022. https://doi.org/10.1016/j.sna.2022.113515

[18] J. Kaur, H. Ghorbanpoor, Y. Öztürk, Ö. Kaygusuz, H. Avcı, C. Darcan, L. Trabzon, F. D. Güzel, On-chip label-free impedance-based detection of antibiotic permeation, IET Nanobiotechnology, 15(1), 100–106, 2021. https://doi.org/10.1049/nbt2.12019

[19] A. Ebrahimi, H. Ghorbanpoor, H. Bagheroghli, N. Lotfibakhshayesh, H. Hashempour, H. Avcı, F. D. Güzel, High-throughput microfluidic chip with silica gel–C18 channels for cyclotide separation, Analytical and Bioanalytical Chemistry, 415(27), 6873–6883, 2023. https://doi.org/10.1007/s00216-023-04966-3